# Transmission electron microscopy and cathodoluminescence of tensile-strained $Ga_xIn_{1-x}P$/InP heterostructures. I. Spatial variations of the tensile stress relaxation

F. Cléton, B. Sieber,[a] and A. Lefebvre
*Laboratoire de Structure et Propriétés de l'Etat Solide, URA CNRS 234, Bâtiment C6, Université des Sciences et Technologies de Lille, 59655 Villeneuve d'Ascq Cedex, France*

A. Bensaada and R. A. Masut
*Groupe de Recherche en Physique et Technologie des Couches Minces, Ecole Polytechnique, C.P. 6218, Montréal, Québec H3C 3A7, Canada*

J. M. Bonard and J. D. Ganière
*IMO, Département de Physique, Ecole Polytechnique Fédérale de Lausanne, CH 1015 Lausanne, Switzerland*

M. Ambri
*Département de Physique des Matériaux, Université Claude Bernard Lyon 1, URA CNRS 172, 43 Boulevard du 11 Novembre 1918, 68622 Villeurbanne Cedex, France*

(Received 15 January 1996; accepted for publication 18 April 1996)

We have investigated the optical and structural properties of tensile-strained $Ga_xIn_{1-x}P$/InP heterojunctions by cathodoluminescence (CL) in the scanning electron microscope and by transmission electron microscopy (TEM). The lattice mismatch of the samples is ranging from 0.4% ($x=5.5\%$) to 0.84% ($x=11.8\%$). We show, in agreement with previous studies, that the relaxation of tensile-strained epilayers occurs by the emission of partial and perfect dislocations. The numerous twins and stacking faults which are found in the epilayers act as efficient recombination centers for electron-hole pairs and appear as dark line defects (DLDs) in CL images. ''Ladderlike'' configurations of these defects are found both by TEM and CL in samples with a lattice mismatch larger than 0.5%. We also demonstrate that DLDs are contaminated by impurities. Areas with networks of perfect dislocations are found between the DLDs. The analysis of the dislocation types allows us to suggest that the growth of low-mismatched samples is two dimensional, and that it is three dimensional in highly mismatched samples. Finally, the spatial variations of the strain relaxation throughout the samples are studied by 77-K CL spectroscopic measurements and it is shown that these variations can be correlated with the various types of structural defects.  [S0021-8979(96)08914-1]

## I. INTRODUCTION

III-V tensile-strained heterostructures[1–13] have been less studied than compressive-strained systems. Nevertheless, the study of such heterostructures is of interest for both fundamental and applied points of view, and more information is still needed for a complete knowledge of their relaxation processes. This paper is a contribution to the study of the relation between the degree of relaxation and the luminescent properties of tensile-strained $Ga_xIn_{1-x}P$/InP heterostructures.

It has been first shown by Marée *et al.*[1] that the relaxation of (001)-oriented tensile-strained systems proceeds in a very different way as compared to (001)-oriented compressive-strained systems. As an illustration of the first difference between the two types of systems, studies on the GaInAs/InP system under tension by means of transmission electron microscopy experiments (TEM) showed the presence of numerous twins and stacking faults in the epilayer due to the propagation of partial dislocations from the surface to the interface[3,4,10] (twins and stacking faults are rarely observed in III-V compressive-strained heterostructures). The presence of such defects in the epilayer is the result of a higher gliding force acting on the 90° leading partial dislocation with respect to that acting on the 30° trailing partial dislocation.[1] The second difference between tensile- and compressive-strained systems is that the relaxation proceeds via partial Ga(g) dislocations—usually named $\beta$ dislocations and oriented along the [110] direction—in the first case, and via As(g) dislocations—$\alpha$ dislocations oriented along the [110] direction—in the second case. Furthermore, cracks in both ⟨110⟩ directions have been detected in tensile-strained systems.[14] The third difference has been noted by Marée *et al.*[1] and concerns the critical thickness which seems to be smaller in tensile-strained systems.

This paper is divided into two parts. Part I deals with the analysis of the strain-relaxation mechanisms in tensile-strained $Ga_xIn_{1-x}P$/InP heterojunctions with a misfit parameter ranging from 0.4%–0.84% and a gallium composition in the range 5.5%–11.8% (Table I). The nature of structural defects has been studied by means of TEM experiments. They are imaged as dark line defects (DLDs) by cathodoluminescence in the scanning electron microscope (SEM/CL). Advantage has been taken of the microresolution of this

[a]Electronic mail: Brigitte.Sieber@univ-lille1.fr

TABLE I. Main characteristics of the (001)-oriented $Ga_xIn_{1-x}P$/InP samples studied in this work. Average gallium composition ($x$), lattice mismatch ($\Delta a/a$) determined from the gallium composition ($x$), strain relaxation $R$ in both $\langle 110 \rangle$ directions, $Ga_xIn_{1-x}P$ and InP epilayer thicknesses $t$. We have also specified on which specimens spectroscopic and/or TEM experiments have been performed.

| Heterojunction | $x_{Ga}$ (%) | $\Delta a/a$ (%) | $R[1\bar{1}0]$ (%) | $R[110]$ (%) | $Ga_xIn_{1-x}P$ epilayer thickness ($\mu$m) | InP buffer layer thickness (nm) | Experiments |
|---|---|---|---|---|---|---|---|
| CD 21S | 5.5 | 0.39 | 4.6 | 7.3 | 1.12 | 100 | SEM/CL imaging +spectroscopy |
| CF 89S | 6.4 | 0.46 | 0.7 | 0.7 | 0.4 | 25 | SEM/CL imaging +spectroscopy +TEM |
| CF 88S | 6.5 | 0.47 | 1.5 | 1.5 | 0.4 | 25 | SEM/CL imaging +spectroscopy +TEM |
| CF 86S | 7.8 | 0.56 | 3.6 | 12.9 | 0.4 | 25 | SEM/CL imaging +spectroscopy |
| CE 62S | 7.6 | 0.54 | 16 | 53 | 1.31 | 200 | SEM/CL imaging |
| CE 83S | 10.6 | 0.75 | 14 | 29 | 0.55 | 25 | SEM/CL imaging +spectroscopy +TEM |
| CE 84S | 11.2 | 0.8 | 13 | 43 | 0.55 | 25 | SEM/CL imaging +spectroscopy +TEM |
| CE 85S | 11.8 | 0.84 | 7 | 50 | 0.55 | 25 | SEM/CL imaging +TEM |

technique to visualize their spatial distribution and to measure, by means of spectroscopic experiments, the spatial distribution of the local relaxation efficiency. We show that variations of the relaxation level induce variations of the luminescence intensity. A detailed analysis of this phenomenon is presented in Part II of the paper. We report in Part II on the combination of spectroscopic CL experiments and semiquantitative analysis of the nondispersive CL signal we have used in order to deduce the origin of the luminescence inhomogeneities in a few $Ga_xIn_{1-x}P$/InP heterojunctions.

## II. EXPERIMENTAL DETAILS

The $Ga_xIn_{1-x}P$ epilayers were grown at 640 °C on (001)-oriented sulfur doped ($n \sim 1\times10^{19}$ cm$^{-3}$) InP substrates using a computer-controlled cold wall horizontal low-pressure MOCVD reactor.[15] Prior to the $Ga_xIn_{1-x}P$ deposition, an InP buffer layer was grown directly on the preheated surface in order to improve the crystallographic quality of the $Ga_xIn_{1-x}P$/InP interface. The nonintentionally doped $Ga_xIn_{1-x}P$ and InP epilayers contained residual impurities ($n=3\times10^{14}$ cm$^{-3}$).[15] The main parameters of the studied specimens are listed in Table I; specimens CE 83S, CE 84S, CE 85S, and CE 62S are considered as highly mismatched samples due to their lattice mismatch value and the thickness of their epilayer. All the other specimens are considered as low-mismatched samples. All the specimens have been characterized by cathodoluminescence imaging in the scanning electron microscope (SEM/CL).

High resolution x-ray diffraction (HRXRD) and low-temperature photoluminescence were used to determine the gallium composition in the epilayers and the degree of relaxation. All the specimens listed in Table I were first observed by plan-view cathodoluminescence images recorded at room temperature on a Cambridge Stereoscan 250 MK3 scanning electron microscope (SEM/CL). The luminescence was detected by either a home-made annular silicon photodiode system located above the specimen which allowed magnifications down to $\times60$, or an Oxford CL system fitted with an ellipsoïdal mirror and a GaAs photocathode which ensured a magnification of about $\times500$. Use of both systems on the same samples allowed us to visualize short- and large-range inhomogeneities of relaxation.

CL spectra were recorded from specific areas at 77 K on a Cambridge S-360 SEM fitted with a Oxford CL system and a Jobin-Yvon HR250 monochromator which allowed a spectral resolution of about 1 meV. Thin foils have also been prepared for a few specimens (Table I) by chemical thinning in a bromide-methanol solution and plan-view TEM observations have been carried out with a Jeol 200 CX electron microscope operated at 200 keV.

## III. NATURE AND DISTRIBUTION OF STRUCTURAL DEFECTS

Before giving the results on highly and low-mismatched samples, we introduce the features which are common to all of them.

### A. Common features

All the $Ga_xIn_{1-x}P$/InP heterojunctions we have observed by plan-view CL exhibit common characteristics. Plan-view CL images shown in Figs. 1(a) and 1(b) reveal that whatever the lattice mismatch, a large number of dark line defects (DLDs) oriented in both $\langle 110 \rangle$ directions are present in the samples. These DLDs correspond to efficient recombination

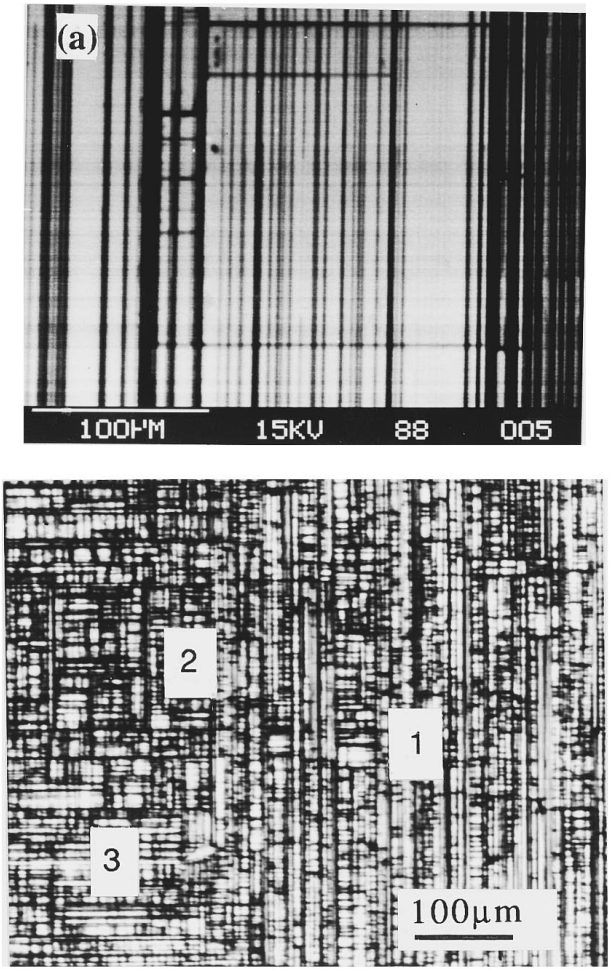


FIG. 1. Typical plan-view SEM/CL images of $Ga_xIn_{1-x}P$/InP heterojunctions, showing the inhomogeneous spatial distribution of DLDs. Photodiodes CL system. $E_0$=15 keV. In these two figures and the following ones, the [110] and [1$\bar{1}$0] directions are, respectively, vertical and horizontal, unless stated otherwise. (a) Low-mismatched sample (CF 88S). The DLDs exhibit various CL contrasts. (b) Highly mismatched sample (CE 83S). In areas labeled 1, 2, and 3, the density of [110] DLDs is, respectively, greater than, equal to, and lower than that of [1$\bar{1}$0] DLDs.

centers which could be groups of either structural defects or point defects. Second, as it can be inferred from the relaxation anisotropy measured by HRXRD (Table I). DLDs nucleation is highly asymmetric. The density of DLDs parallel to the [1$\bar{1}$0] ($\beta$) direction is, in average, higher than that in the [110] ($\alpha$) direction [Figs. 1(a) and 1(b)]. Furthermore, relaxation is inhomogeneous since in a few areas, the [110] DLDs density can equal or exceed the [1$\bar{1}$0] DLDs density [Figs. 1(b)]. Finally, the DLDs are separated by more or less large areas with various CL intensities. These areas, which seem to be free of defects [Figs. 1(a) and 1(b)], are larger and more numerous for low lattice mismatch.

The DLDs are visible at a low value of the accelerating beam energy $E_0$, i.e., when the electron beam penetrates only the epilayer. For instance, Figs. 2(a) and 2(c) show CL pictures of samples CD 21S and CE 89S (Table I) which have been taken for accelerating beam energies values for 5 and 10 keV, respectively; This corresponds to electron penetration depths $R_p$ of 0.16 and 0.5 $\mu$m, as calculated by the Grün formula.[16] The CL images show that the DLDs are visible when the value of the ratio $R_p/t$ ($t$: epilayer thickness) is in the range 1/7 to 1.25. Figures 2(b) and 2(d) show CL pictures of the same areas of CD 21S and CE 89S samples but taken at 25 and 15 keV, respectively. In these cases, the Grün range $R_p$ is equal to 2.7 and 1.1 $\mu$m, respectively. A comparison of Figures 2(a) and 2(b) on the one hand, and of Figs. 2(c) and 2(d) on the other, shows that few DLDs, such as that labeled D on the CL images, are out of contrast when the ratio $R_p/t$ greatly exceeds 1. Therefore, Figs. 2(a)–2(d) show that the number of DLDs detected in the samples by the CL technique depends on the value of the accelerating beam energy $E_0$.[17] This demonstrates the in-depth inhomogeneity of the DLDs distribution. Figure 3 shows that numerous cracks parallel to the [1$\bar{1}$0] direction are also visible in samples from place to place. No cracks in the [110] direction could be observed. This is another proof that relaxation of tensile-strained systems occurs by nucleation of dislocations preferably lying along the [1$\bar{1}$0] direction.

### B. Low-mismatched samples

As shown in Fig. 1(a), DLDs in the [1$\bar{1}$0] direction are generally made of shorter segments than DLDs in the [110] direction. The observation of dark spots by cathodoluminescence at the intersection of both DLD families, such as those labeled $d_s$ in Fig. 3, allows us to suggest that they correspond to dislocations steeply inclined to the surface, as found by CL contrast calculations[18] and experiments.[19] Furthermore, this point has been confirmed by plan-view TEM analysis (see Sec. III C). The CL contrast can be discontinuous along the [1$\bar{1}$0] DLDs (Fig. 3).

The luminescence intensity of the areas located between the DLDs varies from one region to another, and the CL contrast between two areas can be as high as 40%. As shown in Figs. 2(a) and 2(b) as well as in Fig. 4, they can also appear under the form of dark bands. They are oriented in either both $\langle 110 \rangle$ directions [Figs. 2(a) and 2(b)] or only in the [1$\bar{1}$0] direction (Fig. 4).

The CL contrast magnitude and resolution of the defects is DLD dependent. A relation between contrast and resolution can be clearly seen when the DLDs density is low enough as in low-mismatched samples. In Fig. 2(c) for instance, which has been recorded at an accelerating beam energy $E_0$ such that electron-hole pairs are mainly created within the epilayer, the higher the contrast, the lower the resolution. Thus, at least at such an accelerating beam energy, the number of defects which compose one DLD scale with its contrast. Figures 5(a) and 5(b) show that, when a [110] DLD meets a [1$\bar{1}$0] DLD, the DLD contrast can be different on each side of this meeting point. Therefore, it can be suggested that a few [110] DLDs are partially [Fig. 5(a)] or totally [Fig. 5(b)] deviating. As shown in Fig. 5(c), the multiplication of such deviations leads to a ''ladderlike'' configuration which is typical of relaxed $Ga_xIn_{1-x}P$/InP heterostructures. The formation mechanisms of such structures will be described in details in the next section concerning

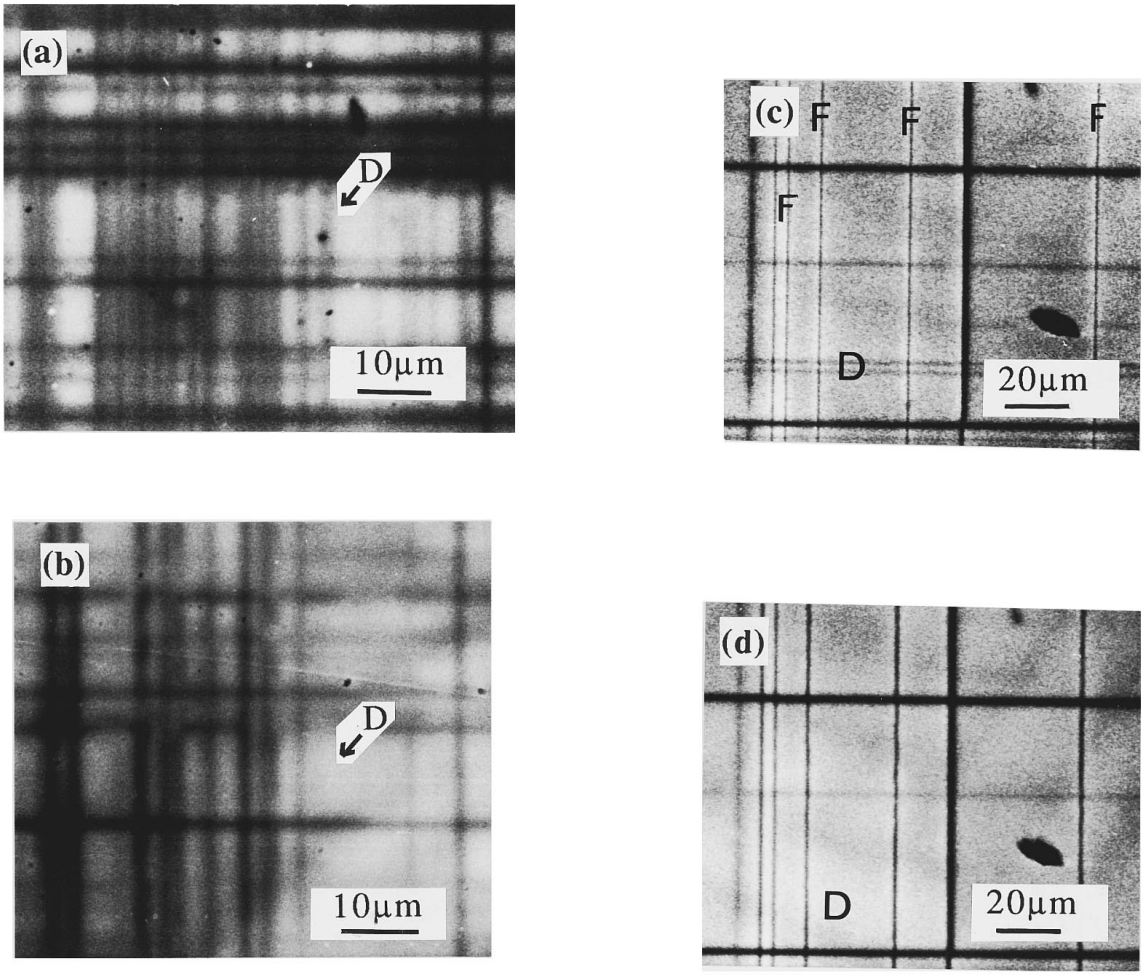


FIG. 2. Low-mismatched samples. Plan-view CL images taken with the Oxford CL system. (a) CD 21S specimen (Table I). The epilayer thickness is 1.12 $\mu$m, $E_0$=5 keV; following Grün,[30] the electron penetration depth $R_p$ is of 0.16 $\mu$m. (b)CD 21S specimen, $E_0$=25 keV, $R_p$=2.7 $\mu$m. (c) CE 89S specimen (Table I). The epilayer thickness is 0.4 $\mu$m, $E_0$=10 keV, $R_p$=0.5 $\mu$m. The bright haloes are clearly seen around DLDs labeled F. (d) CE 89S specimen, $E_0$=15 keV, $R_p$=1.1 $\mu$m. The defects labeled D are out of contrast.

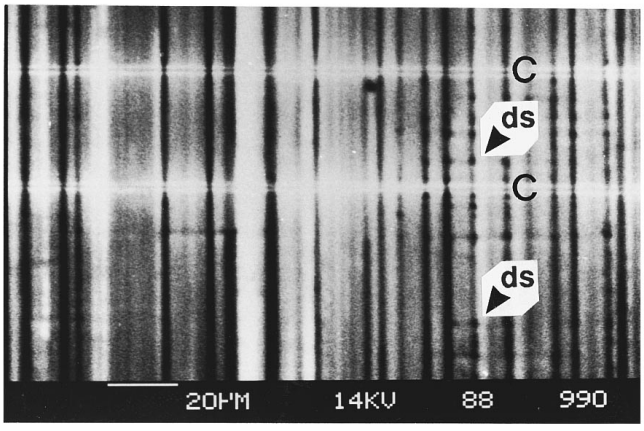


FIG. 3. Plan-view CL image of the CF 88S specimen (Table I) taken with the Oxford CL system. Low-mismatched sample. The epilayer thickness is of 0.4 $\mu$m. $E_0$=14 keV. The dark and bright bands are parallel to the [110] direction. The cracks (labeled C) are parallel to the [110] direction. Following Grün,[30] the electron penetration depth $R_p$ is 1 $\mu$m.

highly mismatched samples since, as a result of their very low density, they have seldom been observed by TEM in low-mismatched samples.

A few ⟨110⟩ DLDs correspond to half-loop defects developed in the substrate and in the interface,[18–20] as illustrated in [Fig. 5(a)]. When observed by TEM, these DLDs were characterized as perfect dislocations.


FIG. 4. Plan-view CL image of the CF 86S specimen (Table I) taken with the Oxford CL system. Low-mismatched sample. The epilayer thickness is of 0.4 $\mu$m, $E_0$=15 keV. Following Grün,[30] the penetration depth $R_p$ is of 1.1 $\mu$m.

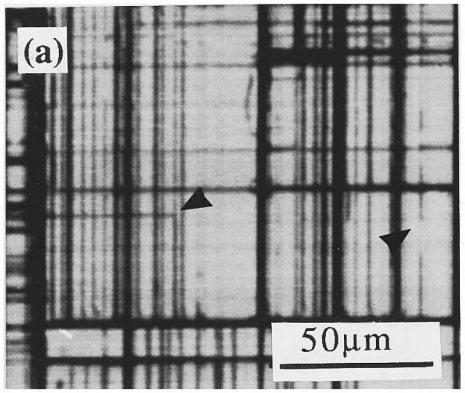


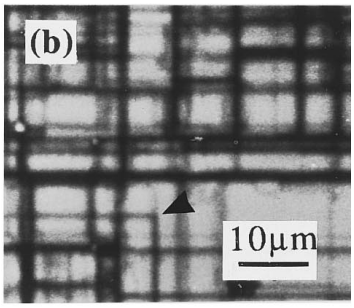


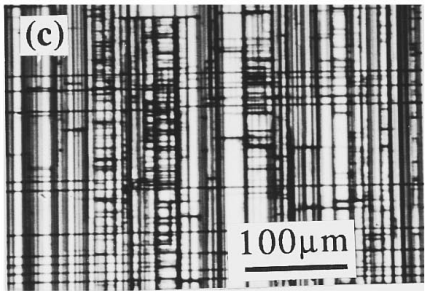


FIG. 5. Plan-view CL images of low-mismatched samples. (a) CF 88S specimen. Photodiode system; $E_0=14$ keV, $R_p=1$ $\mu$m. The partial deviation of a [110] DLD and the half loop DLDs developed in the substrate and in the interface are arrowed. (b) CF 86S specimen. Oxford CL system; $E_0=11$ keV, $R_p=0.64$ $\mu$m. The total deviation of a [110] DLD is arrowed. (c) CF 86S specimen. Picture showing the ''ladderlike'' structure. Photodiode system.

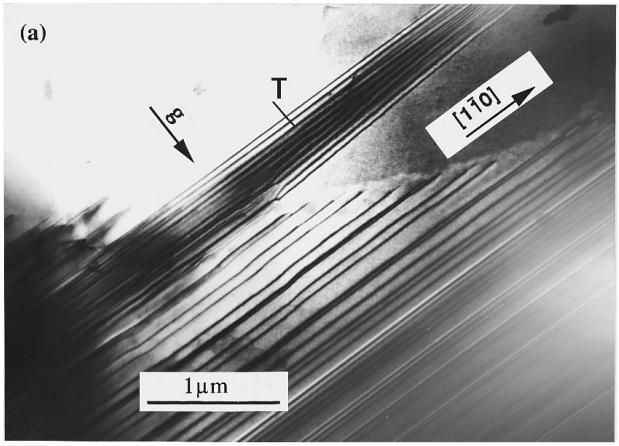


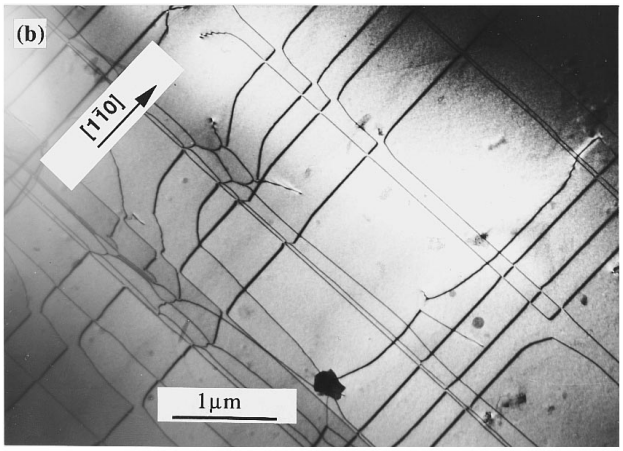


FIG. 6. Plan-view TEM micrograph of the CF 88S specimen (Table I). Low-mismatched sample. (a) Bright field; $g=220$. Dislocations located at the interface are close to the twin labeled T. (b) Bright field; $g=220$. Misfit dislocations network in both ⟨110⟩ directions.

Contamination of the DLDs by impurities is also demonstrated by CL imaging. When imaged at low accelerating beam energies [Fig. 2(c)], DLDs with a low CL contrast (DLDs labeled F) exhibit a bright halo on each side of their dark line. At higher accelerating beam energies [Fig. 2(d)], the same DLDs appear quite wavy. This is typical of impurities segregation at the defect core and the bright halo corresponds to a zone around the defect which is denuded of impurities.[21]

According to the TEM observations, two types of structural defects are found. The first type consists of planar defects (twins, stacking faults) lying in the {111} planes. Figure 6(a) reveals that they generally extend through the $Ga_xIn_{1-x}P$ epilayer. The second type is found not to be connected to the first one. As shown in Fig. 6(b), it consists of an orthogonal array of 60° dislocations lying in the (001) $Ga_xIn_{1-x}P$/InP interface plane and oriented along the [110] and [$1\bar{1}0$] directions [Fig. 6(b)]. The dislocation networks are not very dense and are inhomogeneously distributed throughout the interface. This type of dislocation configuration has been commonly observed in compressive[22,23] and tensile-strained[3,4,10,13] systems. It is characteristic of a two-dimensional growth mode for the epilayer.

### C. Highly mismatched samples

The first striking difference between highly and low-mismatched $Ga_xIn_{1-x}P$/InP heterostructures is the much higher density of DLDs in the former [Fig. 1(b)]. This is in agreement with the higher relaxation levels of highly mismatched samples (Table I). TEM observations show, as illustrated in Fig. 7(a), that most defects parallel to the [110] and [$1\bar{1}0$] directions are, respectively, short intrinsic stacking faults and twins. The stacking faults located in the (111) and ($\bar{1}11$) planes, are confined between the twins as seen in Fig. 7(a). A few twins are also observed in these planes [labeled T2 in Fig. 7(a)]. The stacking faults are thought to be created by a double cross-slip mechanism of partial dislocations in the T1 twins, since these dislocations bounding the stacking faults are systematically found in adjacent T1 twin planes. This is illustrated in Fig. 7(b) in the case of a partial dislo-

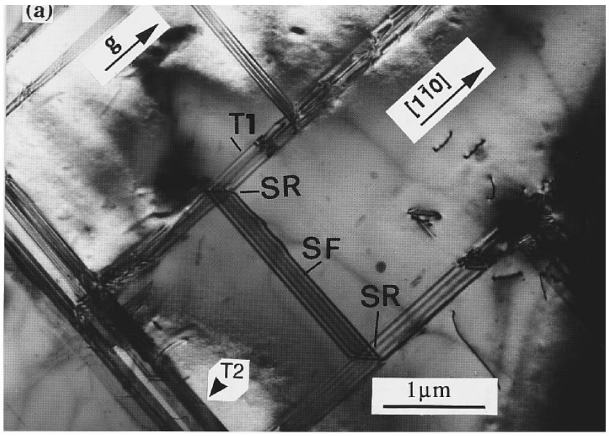


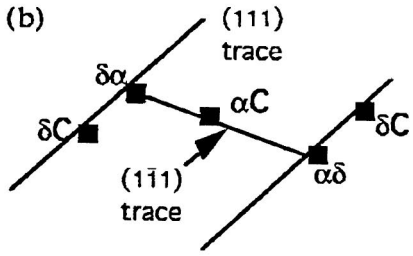


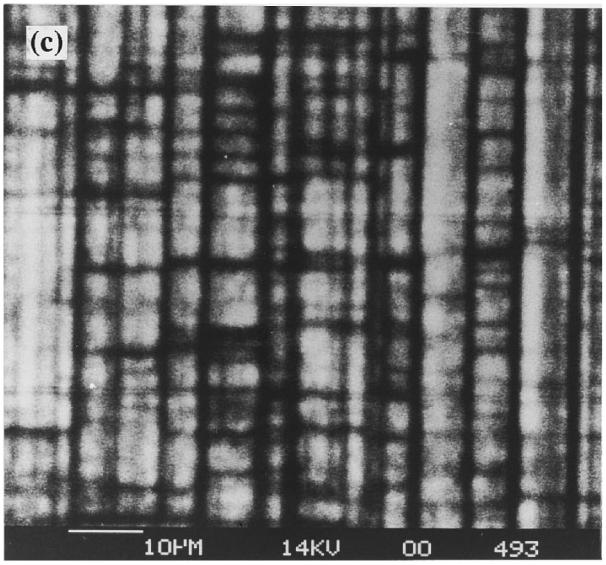


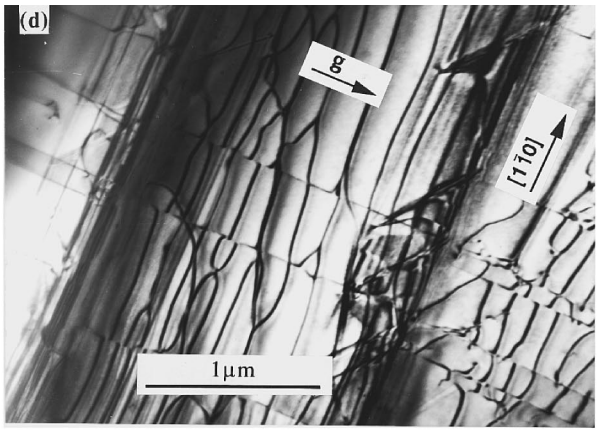


FIG. 7. Highly mismatched structures. CE 84S sample. (a) Plan-view TEM micrograph. Bright field $g=220$. The microtwins (T) and stacking faults (SF) are observed in the epilayer. The stair-rod (SR) dislocations result from cross-slip events. (b) Schematic drawing illustrating the mechanism of double cross-slip which results in the formation of a ''ladderlike'' configuration. See Sec. III C for details. (c) Plan-view CL image showing the ''ladderlike'' structure. Oxford CL system. (d) Plan-view TEM micrograph. Bright field; $g=220$. Dislocation network located at the interface.

cation with 1/6 $[11\bar{2}]$ Burgers vector gliding into the (111) plane. The following reaction is needed for further cross slip into the (111) glide plane:

$$\begin{array}{c} 1/6[11\bar{2}] \rightarrow 1/6[\bar{1}0\bar{1}] + 1/6[21\bar{1}] \\ (\delta C) \quad (\delta\alpha) \quad (\alpha C) \\ (\text{Thompson notation}) \end{array} . \tag{1}$$

The trailing 1/6 $[\bar{1}0\bar{1}]$ stair-rod remains in the T1 twin plane whereas the leading 1/6 [211] Shockley partial can glide into the (111) cross-slip plane in the [110] direction. A single stacking fault is then created in its wake as long as it meets another T1 twin and cross slips in turn. A ''ladderlike'' configuration similar to the one observed by TEM in Fig. 7(a) is then obtained by cathodoluminescence imaging [Fig. 7(c)]. Cross slip of many partial dislocations is at the origin of the presence of T2 twins in the [110] direction [Fig. 7(a)]. The ''ladderlike'' configuration is much more dense in highly than in low-mismatched samples and it extends throughout the sample as seen by CL imaging (Figs. 1 and 5). It is also worth noting that, similarly to low-mismatched samples, areas with more or less bright diffuse CL contrasts remain.

Similarly to low-mismatched samples, a second type of defect not connected with the first one has been identified by TEM observations. Fig. 7(d) reveals that it also consists of inhomogeneously distributed dislocation networks confined at the interface plane, but the dislocations in the [110] direction are of the edge type with a $a/2$ [110] Burgers vector. These dislocations are sheared by perfect 60° dislocations parallel to the [110] direction. This configuration is similar to that observed by Zhu and Carter[24] in GaAs/Si and by Kang *et al.*[25] in GaSb/GaAs heterostructures. The perfect 60° dislocations interact with the sessile edge dislocations which are

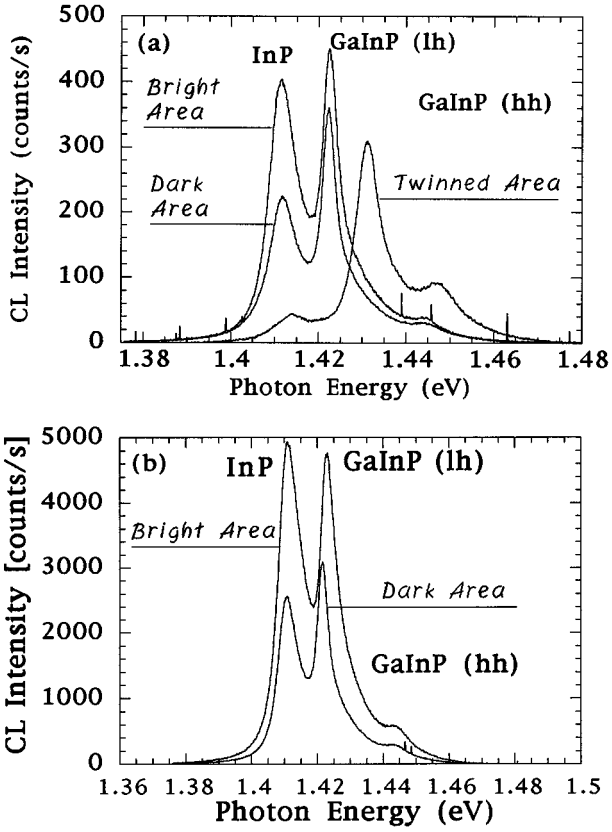


FIG. 8. 77-K CL spectra obtained on three different areas of the CD 21S sample (Table I); $E_0$=10 keV. Low-mismatched sample. (a) Typical CL spectra which show that (i) the twinned area is more relaxed than the adjacent bright and dark areas and (ii) the dark area is slightly more relaxed than the bright area. (b) These spectra show an exception to the rule: the bright area is more relaxed than the dark one.

therefore displaced. This type of interaction is thought to be the result of a three-dimensional growth mode of the epilayer.

The presence of edge dislocations and dense ''ladder-like'' configurations can explain the high relaxation levels found by HRXRD in highly mismatched samples (Table I).

The misfit dislocations which form the networks in both low- and highly mismatched samples are likely to be imaged, by the CL technique, as the diffuse areas noted previously. According to TEM observations [Figs. 6(b) and 7(d)], these dislocations are too close from one to the other to be spatially resolved in the CL mode. Thus, it can be suggested that the brighter the CL intensity, the lower the density of misfit dislocations. In order to validate this hypothesis, which should lead to spatial inhomogeneities in the strain relaxation of the epilayers, we have performed 77-K CL spectroscopic experiments on selected areas in low- and highly mismatched samples. The results we have obtained are presented in the next section.

Our observations, which show that the relaxation of epilayers under tensile strain proceeds via the emission of perfect and partial dislocations, confirm the results obtained by Marée *et al.*[1] and Wagner *et al.*[3,4,10,13] on the InGaAs/InP and InGaP/GaAs systems, respectively.

## IV. SPATIAL VARIATION OF THE RELAXATION LEVEL

Using luminescence measurements alone cannot in principle decouple changes induced by variations in strain relaxation and fluctuations in alloy concentration. In the analysis that follows, we assume that there are no significant changes in the Ga incorporation in the samples presented. This is a reasonable assumption since proton induced x-ray emission line scan analysis of a series of similar samples show no variation of Ga yield, as a function of the beam spot position, to within the precision of this technique.[15]

### A. Low-mismatched samples

The relatively low values of the relaxation levels of low-mismatched samples as measured by HRXRD (Table I), show that the $Ga_xIn_{1-x}P$ epilayer does not undergo a large amount of plastic relaxation. This is confirmed by the results of the CL spectral analysis.

Figures 8(a) and 8(b) show typical CL spectra obtained from a partially relaxed $Ga_xIn_{1-x}P$ layer. The peak which occurs at the lowest energy can be attributed to interband recombination in the InP buffer since its value corresponds to that theoretically expected for undoped InP. The position of the two other peaks can be interpreted, as demonstrated previously,[26] on the basis of the Pikus and Bir theory[27] developed in 1959. The biaxial strain splitting of the $Ga_xIn_{1-x}P$ valence band in a light-hole (lh) and heavy-hole (hh) band leads to the appearance of two conduction band-valence bands (CB-VB) transitions of energy,

$$E_{g\mathrm{hh}}(x;\epsilon)=E_g(x;0)+\Delta E_{\mathrm{hh}}(x;\epsilon), \tag{2}$$

$$E_{g\mathrm{lh}}(x;\epsilon)=E_g(x;0)+\Delta E_{\mathrm{lh}}(x;\epsilon), \tag{3}$$

where $\epsilon(x)$ is the local strain; $E_g(x)$ is the unstrained $Ga_xIn_{1-x}P$ energy band gap; it can be calculated by the following relation (Merle *et al.*[28]) which gives the band-gap energy value of an unstrained $Ga_xIn_{1-x}P$ epilayer as a function of its gallium composition $x$,

$$E_g(x)=E_g(0)+0{,}77x+0{,}684x^2 \quad (x<0{,}8\%), \tag{4}$$

where $E_g(0)$ is the InP band-gap energy expressed, at temperature $T$, by[29]

$$E_g(0)=1{,}4539-0{,}0359\left(1+\frac{2}{e^{209/T}-1}\right) \tag{5}$$

$\Delta E_{\mathrm{lh}}(x;\epsilon)$ and $\Delta E_{\mathrm{hh}}(x;\epsilon)$ are related to $\epsilon(x)$ by

$$\Delta E_{\mathrm{hh}}=\left(-2a\,\frac{c_{11}-c_{12}}{c_{11}}+b\,\frac{c_{11}+2c_{12}}{c_{11}}\right)\epsilon, \tag{6}$$

TABLE II. Elastic stiffness constants of InP and GaP.

| Elastic stiffness constants | $C_{11}$ $10^{10}$ Pa | $C_{12}$ $10^{10}$ Pa | $C_{44}$ $10^{10}$ Pa |
|---|---|---|---|
| InP | 10.22 | 5.76 | 4.6 |
| GaP | 14.12 | 5.25 | 7.05 |

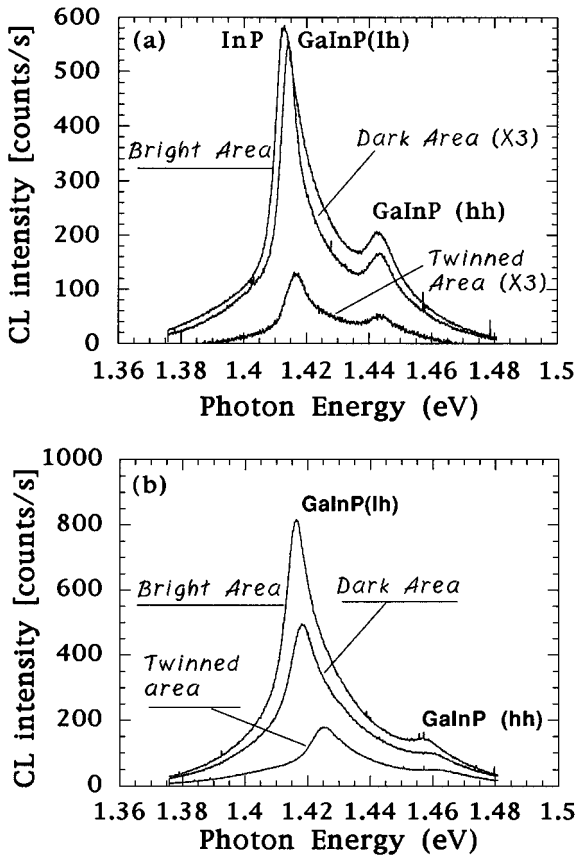


FIG. 9. Typical 77-K CL spectra obtained on low-mismatched samples; $E_0=5$ keV. The InP peak is not visible. The samples are highly strained. (a) CF 88S sample. (b) CF 86 S sample.

$$\Delta E_{\mathrm{lh}}=\left(-2a\,\frac{c_{11}-c_{12}}{c_{11}}-b\,\frac{c_{11}+2c_{12}}{c_{11}}\right)\epsilon-(2b^2/\Delta)\times\left(\frac{c_{11}+2c_{12}}{c_{11}}\right)^2\epsilon^2, \tag{7}$$

where $a$ is the hydrostatic deformation potential and $b$ is the shear deformation potential in the case of deformation with a tetragonal symmetry. $\Delta$ is the spin-orbit splitting between the heavy-hole and the split-off bands. We have taken $a=-1.55$ eV and $b=-2$ eV, $\Delta=108$ meV. We have calculated the elastic stiffness constants $C_{ij}$ of the $Ga_xIn_{1-x}P$ layers by a linear extrapolation of the InP and GaP values reported in Table II. In the above expressions, we have neglected the coupling term between the heavy-hole band and the split-off band. This term does not reduce appreciably the relative displacement of the heavy-hole band.[30] But, as a result of the large value of the coupling term between the light-hole band and the split-off band, we have taken into account the term in $\epsilon^2$ in the expression of $\Delta E_{\mathrm{lh}}$ (this term takes account of a tetragonal deformation). The terms of an order of higher than 2 in $\epsilon$ have been neglected, as well as the term accounting for a rhombohedral deformation.

In the case of a tensile-strained semiconductor, the value of $\epsilon$ is negative, leading to a decrease of the electron-hole pairs transition energies CB-lh and CB-hh with respect to the unstrained material. Furthermore, the CB-lh transition occurs at a lower energy than the CB-hh transition. We can notice that a decrease of the residual strain by a relaxation mechanism leads to an energetical increase (blueshift) by turning back both of the transitions.

Thus, in Figs. 8(a) and 8(b) the CL peaks following that of the InP buffer can be attributed to the CB-lh recombination of electron-hole pairs; the last one—occurring at a higher energy—corresponds to the CB-hh transition. The CL peak positions (lh and hh) yield directly the deformation rate $\epsilon$ which is related to the relaxation level $R$ by

$$\epsilon=(1-R)\Delta a/a. \tag{8}$$

Thus, according to the spectra in Fig. 8(a), relaxation values equal to 10%, 13%, and 33% have been measured for a bright area, dark area, and DLD (twinned area), respectively. These values are rather large, as compared to that derived from HRXRD measurements (Table I). They can be attributed to relaxation inhomogeneities in a relatively thick

TABLE III. Low-mismatched samples. Comparison of the strain relaxations found by 77-K CL spectra and HRXRD.

| Sample | CD 21S $\Delta a/a=0.39\%$ | CE 89S $\Delta a/a=0.46\%$ | CE 88S $\Delta a/a=0.47\%$ | CE 86S $\Delta a/a=0.56\%$ |
|---|---|---|---|---|
| Bright area | 10% | 0% | 0% | 6% |
| Dark area | 13% | 1% | 2% | 7% |
| Twinned area | 33% | 1% | 6% | 18% |
| Average strain relaxation obtained by CL | 18.7% | 0.7% | 2.7% | 10.3% |
| Strain relaxation obtained by CL and by considering 2/3 of bright areas, 1/6 of dark and twinned areas | 14.3% | 0.3% | 1.33% | 8.16% |
| Average strain relaxation obtained by HRXRD | 6% | 0.7% | 1.5% | 8.25% |

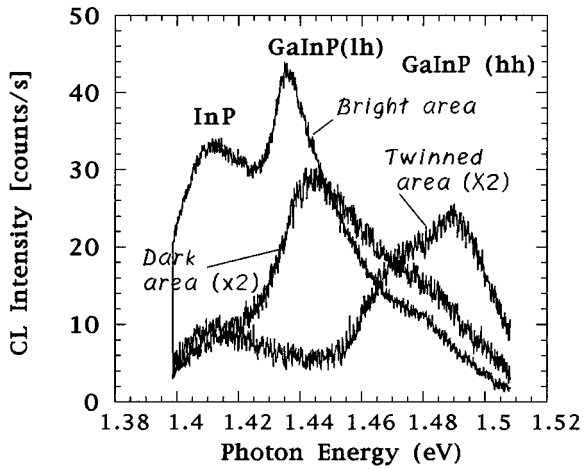


FIG. 10. Typical 77-K CL spectra obtained on a highly mismatched sample CE 84S. $E_0$=5 keV. The InP peak is clearly visible only in the bright area.

sample, as seen by CL imaging. It has been found with a few exceptions [Fig. 8(b)] that the bright areas are more strained than the dark areas.

As far as the three other low-mismatched structures are concerned, the experimental positions of the CL peaks correspond to high residual strain in the $Ga_xIn_{1-x}P$ epilayers in agreement with their thinner thickness (0.4 $\mu$m). The InP buffer layer is so thin in these specimens (250 Å), that the peak related to its luminescence is hidden by the $Ga_xIn_{1-x}P$ (lh) one [Figs. 9(a) and 9(b)].

Relaxation amounts calculated from the CL spectra shown in Fig. 9(a), correspond to the spatially averaged values found in one of the lower-mismatched specimens (CF 88S) by recording many spectra. We can remark that nonrelaxed areas in the epilayer are found in the lower mismatched structures (CF 88S and CF 89S).

For all the low-mismatched samples, except the CF 88S and CF 89S samples, bright and dark areas are thought to be relaxed through the presence of perfect dislocation sources. In all the low-mismatched samples, the intensity of the luminescence originating from strained areas is higher than that issued from more relaxed areas. This seems then to validate our previous hypothesis on the origin of luminescence fluctuations, i.e., that the spatial fluctuations of luminescence observed in the $Ga_xIn_{1-x}P$/InP heterojunctions are the result of variations of the misfit dislocations density. However, as shown in Fig. 8(b), this relation is not always strictly verified, since bright areas can sometimes be more relaxed than dark areas. Thus, a spatial variation of the misfit dislocation density alone cannot account for luminescence fluctuations. They could also be the result of inhomogeneities of the doping level in the epilayer. The detection of CL inhomogeneities in the substrate,[31] related to sulfur doping impurity inhomogeneities, lets us suggest that similar variations in the epilayer have also to be assumed, since they could account for large CL variations. As a matter of fact, the sulfur doping impurities could diffuse from the substrate to the epilayer.[32] Variations of the minority carrier diffusion length could also be responsible for CL intensity fluctuations. The determination of the diffusion-recombination (DR) parameters would allow us to determine exactly the origin of luminescence fluctuations. Such a study is developed in Part II of this paper.

Except for sample CD 21S, the spatial averages of the relaxation values all over the samples are in agreement with the macroscopic values found by HRXRD if we consider twice as many bright areas as dark and twinned ones (Table III). This is the result of the high spatial inhomogeneity of the defects in the samples.

TABLE IV. Highly mismatched samples. Comparison of the strain relaxations found by 77-K CL spectra and HRXRD.

| Sample | CE 83S $\Delta a/a$=0.75% | CE 84S $\Delta a/a$=0.8% |
|---|---|---|
| Bright area | 10% | 20% |
| Dark area | 25% | 30% |
| Twinned area | 25% | 45% |
| Average strain relaxation obtained by CL | 20% | 28% |
| Average strain relaxation obtained by HRXRD | 21.5% | 28% |

### B. Highly mismatched samples

As already observed by HRXRD (Table I), the highly mismatched samples are more relaxed than the low-mismatched ones. CL spectra shown in Fig. 10 reveal that, in these structures, all the bright, dark and twinned areas are notably relaxed. The measured relaxation values are consistent with a high density of perfect interfacial dislocations in these areas. They are also in agreement with the large twin thicknesses observed in the corresponding areas.

If we consider as many bright, dark, and twinned areas, spatial averages of the relaxation values all over the samples give the same result than that found by HRXRD (Table IV). This shows that the distribution of defects is, in contrast to low-mismatched samples, more homogeneous in these samples.

## V. CONCLUSION

In this paper we have shown that low- and highly mismatched $Ga_xIn_{1-x}P$/InP structures exhibit common characteristics in their relaxation mechanisms. Except for a few cracks along the [110] direction, many [110] twins allow an effective local relaxation of the epilayer. The number of twins increases with lattice mismatch; this leads, by cross-slip events, to the presence of stacking faults or twins along the [110] direction. The resulting ''ladderlike'' structure of defects are observed by TEM and CL. In parallel, the analysis of perfect interfacial dislocation networks which develop simultaneously with partial dislocations, allow us to suggest that heteroepitaxial growth of the low- and highly mismatched heterostructures are, respectively, of a two- and three-dimensional type.

Spatial luminescence fluctuations observed all over both types of structures are likely to be connected with inhomogeneities of misfit dislocation since most of the 77 K CL spectra are such that the luminescence intensity of the more relaxed areas is lower than in more strained areas.

## ACKNOWLEDGMENTS

C. Vanmansart is greatly acknowledged for the building of the silicon photodiode device. Many thanks are also due B. Hue for mechanical assistance and to L. Isnart and R. Lacoursière for technical assistance in MOCVD. This research was partially supported by NSERC (Canada) and FCAR (Québec) research grants.

[1] P. M. J. Marée, J. C. Babour, J. F. Van der Veen, K. L. Kavanagh, C. W. T. Bulle-Lieuwma, and M. P. A. Viegers, J. Appl. Phys. **62**, 4413 (1987).
[2] N. G. Chew, A. G. Cullis, S. J. Bass, L. L. Taylor, M. S. Skolnick, and A. D. Pitt, Inst. Phys. Conf. Ser. **87**, 231 (1987).
[3] G. Wagner, P. Paufler, and G. Rohde, Z. Krist. **189**, 269 (1989).
[4] G. Wagner, V. Gottschalch, H. Rhan, and P. Paufler, Phys. Status Solidi A **112**, 519 (1989).
[5] C. Frigeri, G. Attolini, C. Pelosi, and R. Gleichmann, Mater. Sci. Eng. B **9**, 115 (1991).
[6] D. M. Hwang, S. A. Schwarz, R. Bhat, and C. Y. Chen, Inst. Phys. Conf. Ser. **120**, 365 (1991).
[7] D. M. Hwang, S. A. Schwarz, T. S. Ravi, R. Bhat, and C. Y. Chen, Phys. Rev. Lett. **66**, 739 (1991).
[8] D. M. Hwang, R. Bhat, S. A. Schwarz, and C. Y. Chen, Mater. Res. Soc. Symp. Proc. **263**, 421 (1992).
[9] H. H. Park, K. H. Lee, J. L. Lee, Y. T. Lee, E-H. Lee, J. Y. Lee, S. K. Hong, and O. D. Kwon, J. Appl. Phys. **72**, 4063 (1992).
[10] G. Wagner and P. Paufler, Phys. Status Solidi A **138**, 389 (1993).
[11] J. Wang, J. W. Steeds, and M. Hopkinson, Semicond. Sci. Technol. **8**, 502 (1993).
[12] W. Wegscheider and H. Cerva, J. Vac. Sci. Technol. B **11**, 1056 (1993).
[13] G. Wagner, V. Gottschalch, R. Franzheld, S. Kriegel, and P. Paufler, Phys. Status Solidi A **146**, 371 (1994).
[14] A. Antolini, C. Papuzza, G. Schiavini, D. Soldani, F. Taiariol, L. Lazzarini, G. Salviati, M. Mazzerand, and C. Zanotti-Fregonara, Inst. Phys. Conf. **146**, 365 (1995).
[15] A. Bensaada, A. Chennouf, R. W. Cochrane, R. Leonelli, P. Cova, and R. A. Masut, J. Appl. Phys. **71**, 1737 (1992); A. Bensaada, R. W. Cochrane, R. A. Masut, R. Leonelli, and G. Kajrys, J. Cryst. Growth **130**, 433 (1993).
[16] A. E. Grün, Z. Naturforsh. **12a**, 89 (1957).
[17] F. Cléton, B. Sieber, A. Bensaada, L. Isnart, and R. A. Masut, Inst. Phys. Conf. **134**, 655 (1993).
[18] C. Donolato and H. Klann, J. Appl. Phys. **51**, 1624 (1980).
[19] Z. J. Radzimski, B. L. Jiang, G. A. Rozgonyi, T. P. Humphreys, N. Hamaguchi, and S. M. Bedair, J. Appl. Phys. **64**, 2328 (1988).
[20] O. Ueda, Mater. Sci. Eng. B **20**, 9 (1993).
[21] G. R. Booker, Inst. Phys. Conf. Ser. **60**, 203 (1981).
[22] C. Herbeaux, J. Di Persio, and A. Lefebvre, Appl. Phys. Lett. **54**, 1004 (1989).
[23] C. Ulhaq-Bouillet, A. Lefebvre, and J. Di Persio, Philos. Mag. A **69**, 995 (1994).
[24] J. G. Zhu and C. B. Carter, Philos. Mag. **62**, 319 (1990).
[25] J. M. Kang, M. Nouaoura, L. Lassabatère, and A. Rocher, J. Cryst. Growth **143**, 115 (1994).
[26] A. Bensaada, A. Chennouf, R. W. Cochrane, J. T. Graham, R. Leonelli, and R. A. Masut, J. Appl. Phys. **75**, 3024 (1994).
[27] G. E. Pikus and G. L. Bir, Sov. Phys. Solid State **1**, 136 (1959).
[28] P. Merle, D. Auvergne, H. Mathieu, and J. Chevallier, Phys. Rev. B **15**, 2032 (1977).
[29] L. Pavesi, F. Piazza, A. Rudra, J. F. Carlin, and M. Ilegems, Phys. Rev. B **44**, 9052 (1991).
[30] J. Y. Marzin, M. N. Charasse, and B. Sermage, Phys. Rev. B **31**, 8298 (1985).
[31] F. Cléton (unpublished).
[32] A. Bensaada, R. W. Cochrane, and R. A. Masut, Proceedings of the 6th International Conference on Indium Phosphide and Related Materials, IEEE, Catalog No. 94CH3369-6, March 1994, Santa Barbara, CA, pp. 118–121.